HHS Public Access

Author manuscript

Nature. Author manuscript; available in PMC 2019 December 13.

Published in final edited form as:

Nature. 2019 April ; 568(7753): 541–545. doi:10.1038/s41586-019-1105-7.

Developmental origin, functional maintenance and genetic rescue of osteoclasts

Christian E. Jacome-Galarza[1,7], **Gulce I. Percin**[2,3,7], **James T. Muller**[1,7], **Elvira Mass**[1,6,7], **Tomi Lazarov**[1], **Jiri Eitler**[2], **Martina Rauner**[4], **Vijay K. Yadav**[5], **Lucile Crozet**[1], **Mathieu Bohm**[1], **Pierre-Louis Loyher**[1], **Gerard Karsenty**[5], **Claudia Waskow**[2,3,4,8], **Frederic Geissmann**[1,8]

[1]Immunology Program, Sloan Kettering Institute, Memorial Sloan Kettering Cancer Center, New York, NY, USA.

[2]Regeneration in Hematopoiesis and Animal Models in Hematopoiesis, Institute for Immunology, Dresden, Germany.

[3]Regeneration in Hematopoiesis, Leibniz Institute on Aging—Fritz Lipmann Institute (FLI), Faculty of Biological Sciences, Friedrich-Schiller University, Jena, Germany.

[4]Department of Medicine III, Faculty of Medicine, Dresden, Germany.

[5]Department of Genetics and Development, Columbia University Medical Center, New York, NY, USA.

[6]Present address: Developmental Biology of the Innate Immune System, LIMES Institute, University of Bonn, Bonn, Germany.

[7]These authors contributed equally: Christian E. Jacome-Galarza, Gulce I. Percin, James T. Muller, Elvira Mass.

[8]These authors jointly supervised this work: Claudia Waskow, Frederic Geissmann.

Abstract

* geissmaf@mskcc.org.

Author contributions F.G. and C.W. designed the study, supervised experiments and analysed data. F.G. wrote the draft of the manuscript. C.E.J.-G. performed histology and immunofluorescence analyses. E.M. and C.E.J.-G. supervised or performed fate-mapping and genetic deletion experiments with *Csf1r*$^{Mer\text{-}iCre\text{-}Mer}$, *Flt3*^{Cre}, *Csf1r*^{iCre} and *Tnfrsf11a*^{Cre}, EdU incorporation studies and adoptive transfer studies. G.I.P. performed lineage tracing and genetic deletion experiments with *Tnfrsf11a*^{Cre} and *Vav*^{Cre} mice and histomorphometry studies. J.T.M. performed and analysed rescue experiments in *Catk*-deficient mice and *Csf1r*^{Cre};*Csf1r*$^{f/f}$ *mice*. P.-L.L. assisted with parabiosis surgeries. V.K.Y. and G.K. analysed *Catk* parabiosis rescue experiments. J.E. performed inducible genetic deletion experiments in *R26-CreER*$^{T2+}$;*Csf1r*$^{F/F}$ embryos. T.L., L.C., G.I.P., M.B. and E.M. performed flow cytometry analyses. M.R. scanned bones using micro-CT, and M.R. and G.I.P. analysed micro-CT data. All authors contributed to the manuscript.

Competing Interests F.G. is a consultant and principal investigator on a Sponsored Research Agreement with Third Rock Venture (TRV). The other authors declare no competing interests.

Additional Information

Publisher's note: Springer Nature remains neutral with regard to jurisdictional claims in published maps and institutional affiliations.

Online content

Any methods, additional references, Nature Research reporting summaries, source data, statements of data availability and associated accession codes are available at [DOI link]

Osteoclasts are multinucleated giant cells that resorb bone, ensuring development and continuous remodelling of the skeleton and the bone marrow haematopoietic niche. Defective osteoclast activity leads to osteopetrosis and bone marrow failure[1–9], whereas excess activity can contribute to bone loss and osteoporosis[10]. Osteopetrosis can be partially treated by bone marrow transplantation in humans and mice[11–18], consistent with a haematopoietic origin of osteoclasts[13,16,19] and studies suggesting that they develop by fusion of monocytic precursors derived from haematopoietic stem cells in the presence of CSF1 and RANK ligand[1,20]. However, the developmental origin and lifespan of osteoclasts, and the mechanisms that ensure maintenance of osteoclast function throughout life in vivo remain largely unexplored. Here we report that osteoclasts that colonize fetal ossification centres originate from embryonic erythro-myeloid progenitors[21,22]. These erythro-myeloid progenitor-derived osteoclasts are required for normal bone development and tooth eruption. Yet, timely transfusion of haematopoietic stem cells derived monocytic cells in newborn mice is sufficient to rescue bone development in early-onset autosomal recessive osteopetrosis. We also found that the postnatal maintenance of osteoclasts, bone mass and the bone marrow cavity involve iterative fusion of circulating blood monocytic cells with long-lived osteoclast syncytia. As a consequence, parabiosis or transfusion of monocytic cells results in long-term gene transfer in osteoclasts in the absence of haematopoietic stem cell chimerism, and can rescue an adult-onset osteopetrotic phenotype caused by cathepsin K deficiency[23,24]. In sum, our results identify the developmental origin of osteoclasts and a mechanism that controls their maintenance in bones after birth. These data suggest new strategies to rescue osteoclast deficiency in osteopetrosis and to modulate osteoclast activity in vivo.

In vitro, osteoclasts arise by fusion of haematopoietic stem cell (HSC)-derived precursors and require expression of *Csf1r* and *Tnfrsf11a* (also known as *Rank*). To probe the origin of osteoclasts in vivo we first generated $Csf1r^{Cre}$;$Csf1r^{fl/fl}$ and $Csf1r^{Cre}$;$Tnfrsf11a^{fl/fl}$ mice. These mice presented with an osteopetrotic phenotype similar to $Csf1^{op/op}$ (ref. 5), $Csf1r^{6}$ and $Tnfrsf11a^{3}$ mutants, characterized in young mice by lack of teeth eruption, skull and skeletal deformities with shortness of long bones, increased bone density, and lack of osteoclasts and haematopoietic cells (Fig. 1a, Extended Data Fig. 1). To confirm that osteoclast differentiation requires expression of *Tnfrsf11a* and *Csf1r* in HSC-derived precursors, we generated $Flt3^{Cre}$;$Tnfrsf11a^{fl/fl}$, $Flt3^{Cre}$;$Csf1r^{fl/fl}$ and $Vav1^{Cre}$;$Csf1r^{fl/fl}$ mice. Surprisingly, the young mutant mice had normal teeth, bone morphology, bone marrow cellularity and osteoclast numbers in comparison to control littermates (Fig. 1b–d, Extended Data Fig. 2). However, $Flt3^{Cre}$;$Tnfrsf11a^{fl/fl}$, $Flt3^{Cre}$;$Csf1r^{fl/fl}$ and Vav^{Cre};$Csf1r^{fl/fl}$ mice lost their osteoclasts over time (Fig. 1d), and by 22–60 weeks of age had increased trabecular bone density (Fig. 1e) and decreased haematopoietic cell numbers in the long bones (Fig. 1c, Extended Data Fig. 2), and 3D X-ray imaging by micro-computed tomography (micro-CT) confirmed the increased bone mass, whereas bone formation—measured by calcein incorporation—was similar to that in control mice (Fig. 1f, Extended Data Fig. 3). In addition, tartrate resistant acid phosphatase-positive ($TRAP^{+}$) multinucleated cells that appear at embryonic day (E)15 in ossification centres[25] in $Csf1r^{Cre}$;$Rosa26^{LSL\text{-}YFP}$ mice were labelled with YFP, and osteoclasts remained YFP-positive throughout life (Fig. 1g, Extended Data Fig. 4), but gained expression of YFP after birth in $Flt3^{Cre}$;$Rosa26^{LSL\text{-}YFP}$ mice despite colonization of the fetal bone marrow by $Flt3^{Cre+}$ YFP^{+} haematopoietic cells (Fig. 1h, Extended Data Fig. 4).

These data suggested that although postnatal contribution of HSC-derived cells is important for optimal osteoclast maintenance and function in adults and ageing mice, osteoclast development, tooth eruption and the development of bone and the bone marrow cavity require precursors that are independent from the HSC lineage. These precursors may originate from the embryonic erythro-myeloid progenitor (EMP) lineage of resident macrophages[22,26,27], because *Csf1r*^{Cre} mice enable deletion of target genes in both the embryonic EMP lineage and in the HSC lineage, whereas *Flt3*^{Cre} and *Vav*^{Cre} (Extended Data Fig. 5) are not expressed in the EMP lineage. In support of this hypothesis, we found that TRAP^{+} multinucleated cells develop in ossification centres from *Myb*-deficient embryos around E15; at this stage the embryos lack HSCs but still support the development of EMP-derived macrophages[26] (Fig. 2a, b). In addition, TRAP^{+} multinucleated cells are labelled with YFP in tamoxifen-inducible *Csf1r*$^{Mer\text{-}iCre\text{-}Mer}$;*Rosa26*$^{LSL\text{-}YFP}$ mice pulsed at E8.5 with a single dose of hydroxytamoxifen (4-OHT), which labels EMPs but not HSCs[22,26,27] (Fig. 2c, d, Extended Data Fig. 4). Together, these results indicate that fetal osteoclasts arise from EMPs in ossification centres.

We therefore investigated whether EMPs are required for bone development. *Tnfrsf11a* is expressed by osteoclasts, but its expression is also a hallmark of EMP-derived macrophage precursors that colonize the developing embryo[27]. In two independent lines of *Tnfrsf11a*^{Cre} knock-in mice, referred to as ‘Koba’ and ‘Wask’(Fig. 2e–j), Cre-mediated expression of a *Rosa26*$^{LSL\text{-}YFP}$ fluorescent reporter occurs with high efficiency in fetal macrophages but with low efficiency[27] or not at all[28] in HSCs and their progeny in blood and tissues[27,28] (Extended Data Fig. 5). We therefore hypothesized that conditional deletion of *Csf1r* in *Tnfrsf11a*^{Cre} mice would recapitulate the macrophage deficiency observed in *Csf1r*-deficient mice[6], while leaving the HSC lineage unaffected. To test osteoclast and bone development in this model, we generated *Tnfrsf11a*^{Cre};*Csf1r*$^{fl/fl}$ mice (Fig. 2e–j). *Tnfrsf11a*^{Cre};*Csf1r*$^{fl/fl}$ mice lacked tissue macrophages such as brain microglia and epidermal Langerhans cells at birth, whereas development of HSCs and blood cells was preserved (Extended Data Fig. 2). They exhibited a severe osteopetrotic phenotype, including a lack of tooth eruption (Fig. 2e), misshaped skulls and shorter long bones (Fig. 2f–h, Extended Data Fig. 1) with few osteoclasts (Fig. 2i) and increased bone density, and initially lacked a bone marrow cavity (Fig. 2f, Extended Data Fig. 2). In contrast to *Csf1r*-deficient mice, however, osteoclasts and haematopoietic cells progressively colonized the long bones of *Tnfrsf11a*^{Cre};*Csf1r*$^{fl/fl}$ mice during the first month of life (Fig. 2i, Extended Data Figs. 1, 2), although the mice remained toothless and skull and long-bone deformity persisted (Fig. 2e–h, Extended Data Fig. 1). Calcein incorporation was similar in *Tnfrsf11a*^{Cre};*Csf1r*$^{fl/fl}$ mice and their littermate controls (Extended Data Fig. 6). In a complementary approach, ablation of *Csf1r* expression in E10.5 embryos using a single dose of tamoxifen in *Rosa26-creER*$^{T2+}$;*Csf1r*$^{fl/-}$ mice resulted in defective tooth eruption in three out of four pups at 21 days of age (Extended Data Fig. 5). Together, these analyses support a model in which EMP-derived embryonic osteoclasts are needed for teeth eruption, normal skull shape, optimal formation of long bones and the timely colonization of long bones by haematopoietic progenitors, whereas HSC-derived osteoclasts are important for the maintenance of bone mass after birth and later in life, although they may partially rescue bone development in the absence of EMP-derived osteoclasts in *Tnfrsf11a*^{Cre};*Csf1r*$^{fl/fl}$ mice.

To probe the mechanisms that underlie the contribution of HSC-derived blood cells to osteoclast maintenance as well as the lifespan and dynamics of osteoclasts in vivo, we performed time-course parabiosis experiments (Fig. 3a). After four to eight weeks of shared blood circulation between *Csf1r*^{Cre};*Rosa26*$^{LSL\text{-}YFP}$ and *Csf1r*^{Cre};*Rosa26*$^{LSL\text{-}tdTomato}$ parabionts, all osteoclasts, defined as TRAP^{+} multinucleated cells lining the bone surface, expressed both YFP and tdTomato (Fig. 3a, b). No other cell type was found to co-express YFP and tdTomato in bones (Fig. 3b). This is consistent with the presence of nuclei from both partners in individual osteoclasts. Moreover, when parabionts were separated after four weeks (Fig. 3c), most recipient YFP^{+} osteoclasts retained tdTomato staining 14 weeks after separation, and two thirds of osteoclasts from former parabionts still expressed both YFP and tdTomato 24 weeks after separation (Fig. 3c). TdTomato signal intensity per YFP osteoclast increased during the eight-week period of shared blood circulation, and decreased after separation (Extended Data Fig. 7). Most mouse osteoclasts contained around five (range from three to seven) nuclei, with a modest increase of nuclei number per cell between one and six months of age (Fig. 3d). These data therefore suggest that individual osteoclast syncytia are long lived, but acquire new nuclei one at a time every four to eight weeks, from circulating blood cells; it therefore takes more than six months to renew all five nuclei in an individual osteoclast.

We calculated the number and fusion rate of HSC-derived nuclei acquired by osteoclasts in short-term 5-ethynyl-2′-deoxyuridine (EdU)-incorporation studies. A single intravenous pulse of EdU (20 μg g^{-1}) labelled mitotic nuclei and was bioavailable in the bone marrow for around 90 min; approximately 50% of bone marrow and blood monocytic cells were EdU^{+} for around 48 h (Extended Data Fig. 7). We observed that approximately 1–2% of osteoclasts were labelled after 72 h, with only one EdU^{+} nucleus per osteoclast in 90% of EdU^{+} cells (Fig. 3e), suggesting that osteoclasts acquire a single post-mitotic nucleus at a time. In this model, 0.5–2% of osteoclasts per day acquire a new nucleus, compatible with individual nuclei being replaced about every two months. Together, these studies suggest a model (Fig. 3f) in which osteoclasts that control skeletal development mature in ossification centres from EMPs, whereas their post-natal maintenance is mediated by the serial acquisition by long-lived syncytia of new nuclei from HSC-derived blood leukocytes, rather than by de novo renewal by lateral fusion or proliferation of osteoclast precursors.

A prediction from this model, consistent with an early observation[29], is that osteopetrosis due to a recessive mutation affecting osteoclast function may be rescued or prevented through parabiosis with a wild-type partner. Parabiosis experiments between four-week-old cathepsin K-deficient mice, which develop an adult-onset form of osteopetrosis known as pycnodysostosis[23,24], and cathepsin K$^{+/-}$ or cathepsin K$^{-/-}$ littermates, and between wild-type mice as control, showed a reduction of bone volume in ten-week-old cathepsin K$^{-/-}$ mice paired with cathepsin K$^{+/-}$ littermates (Fig. 4a), suggesting that circulating blood cells carrying a wild-type cathepsin K allele are sufficient to reduce bone density. To confirm that expression of a donor-derived gene by recipient osteoclasts results from fusion with monocytic cells circulating in the blood, we performed intravenous injections of KIT^{-}LY6C^{+} cells from the bone marrow of *Csf1r*^{Cre};*Rosa26*$^{LSL\text{-}tdTomato}$ mice into *Csf1r*^{Cre};*Rosa26*$^{LSL\text{-}YFP}$ recipients (Fig. 4b, Extended Data Fig. 8). This resulted in stable expression of tdTomato in 20–40% of osteoclasts one week and eight weeks after

transfusion, in the absence of other donor-derived blood cells or bone marrow progenitors (Fig. 4b, c, Extended Data Fig. 8). These results suggest that parabiosis or an appropriate transfusion protocol can achieve expression of a donor-derived gene by recipient osteoclasts in the absence of HSC chimerism, and that this effect can last several months.

Partial rescue of osteopetrosis occurs postnatally in *Tnfrsf11a*^{Cre};*Csf1r*$^{fl/fl}$ mice, suggesting that transfusion of monocytic cells may also be able to rescue bone development in early-onset congenital osteopetrosis in the absence of a bone marrow transplantation. Intra-peritoneal injections of KIT^{-}LY6C^{+} monocytic cells from *Csf1r*^{Cre};*Rosa26*$^{LSL\text{-}YFP}$ mice into *Csf1r*^{Cre};*Csf1r*$^{F/F}$ neonates, starting from post-natal day (P)5, resulted in complete or partial rescue of teeth eruption (Fig. 4d) and long bone development as assessed by computerized tomography (CT) scan, with the development of a bone marrow cavity (Fig. 4d) at day 14 in infant mice from three different litters (Fig. 4d, Extended Data Fig. 9). In these mice, femur histology indicated the presence of numerous YFP^{+}TRAP^{+} osteoclasts lining the bone (Fig. 4e, f). Histology and flow cytometry analyses showed the lack of YFP^{+} circulating blood cells or bone marrow progenitors (Fig. 4e, g), indicating the absence of HSC engraftment. These data suggest that transfusion of monocytic cells can rescue bone development in early-onset autosomal recessive osteopetrosis in infant mice, in the absence of HSC transplantation.

In sum, we have shown here that osteoclasts originating from EMPs are essential for normal bone development. Moreover, we show that osteoclasts are long-lived in adults and that their function is maintained by iterative fusion of individual HSC-derived circulating cells with existing syncytia. With absence or deficiency of EMP-derived osteoclasts however, their timely replacement by transfusion with monocytic cells can rescue bone development in early-onset osteopetrotic mice without bone marrow transplantation. This is of potential clinical relevance because bone marrow and HSC transplantation, the standard treatment for early-onset osteopetrosis in mice and humans[11–18], requires irradiation or chemotherapy—which increases the risk of infections, is frequently performed in patients who already suffer severe complications, and has a six-year overall survival rate of approximately 48%[17]. In addition, the original mechanism that mediates osteoclast maintenance in adult mice suggests that these cells represent a unique target for gene transfer by cellular therapies based on transfusion of wild-type or engineered monocytic cells to modulate osteoclast activity and bone remodelling in adults.

Extended Data

Extended Data Table 1.

Mouse genotyping

Mouse line		Primer 1 sequence 5' --> 3'	Primer 2 sequence 5' --> 3'	Denaturation	Annealing	Elongation	Cycles	Final Enlongation	Expected bands
Csf1r^{iCre}	Mutant allele	TCTCTGCCCAGAGTCATCCT	CTCTGACAGATGCCAGGACA	94°C – 45sec	60°C – 45sec	72°C – 45sec	30	72°C – 5 min	Mutant: 400 bp
Csf1r^{MeriCreMer}	WT allele Mutant allele	TCGAAGCTTGCATGCCTGCA TCATTCCAGAACCAGAGC	TCTCTGCCCAGAGTCATCCT GATCGTGTTGGGGAAGCC	94°C – 45sec	60°C -90sec	72°C – 90sec	30	72°C – 5 min	WT: 1Kb Mutant: 2 Kb
Cff1r^{flox}	Mutant allele	GCCACCAT GTGTCCGTG CTT	ACCCAGAGCCCCCACAGATA	94°C – 30sec	60°C – 60sec	72°C – 60sec	35	72°C – 2 min	WT: 450 bp Floxed: 500 bp

Mouse line		Primer 1 sequence 5' --> 3'	Primer 2 sequence 5' --> 3'	Denaturation	Annealing	Elongation	Cycles	Final Enlongation	Expected bands
Cffir$^{+/-}$	Mutant allele	GGT GGAT GT G GAAT GTGTGCG	CGTTTCTTGTGGTCAGGGTGC	95°C – 20sec	62°C – 20sec	72°C – 40sec	35	72°C – 5 min	Mutant: 314
Flt3Cre	Mutant allele	ACGGAGTCCAGGCAACTTCC	GAAGCATGTTTAGCTGGCCC	94°C – 30sec	58°C – 35sec	68°C – 60sec	44	72°C – 2 min	Mutant: 400 bp
Myb$^{+/-}$	WT allele Mutant allele	CCATGCGTCGCAAGGTGGAAC CCATGCGTCGCAAGGTGGAAC	GTGCTTCGGCGATGTGGTAA TGGCCGCTTTTCTGGATTCATC	94°C – 30sec	60°C – 30sec	72°C – 60sec	35	72°C – 7 min	WT: 200 bp Mutant: 300 bp
Rosa26CreERT2	Mutant allele	GCCTGCATTACCGGTCGATGCAACGA	AATGGTGTTGCCGCGCCATCTGCCAC	95°C – 20sec	67°C – 20sec	72°C – 50sec	40	72°C – 2 min	Mutant: 700bp
Rosa26LSL-yFP	WT allele Mutant allele	AAGTCGCTCTGAGTTGTTAT AAGTCGCTCTGAGTTGTTAT	GGAGCGGGAGAAATGGATATG GCGAAGAGTTTGTCCTCAACC	94°C – 40sec	60°C – 60sec	72°C – 60sec	34	72°C – 5 min	WT: 525 bp Mutant: 300 bp
Rosa26LSL-tdTornato	WT allele	AAGGGAGCTGCAGTGGAGTA	CCGAAAATCTGTGGGAAGTC	Step 1: 94°C – 20sec	65°C – 15sec (0.5C decrease per cycle) 60°C – 15sec	68°C – 10sec	10	72°C – 2 min	WT: 297 bp
	Mutant allele	GGCATTAAAGCAGCGTATCC	CTGTTCCTGTACGGCATGG	Step 2: 94°C – 15sec	60°C – 15sec	72°C – 10sec	28		Mutant: 196 bp
Tnfrff11aflox	WT allele	AGTGTGCCTGGCATGTGCAGACCTT	CTGGTGGTTGTTCTCCTGGTGTCAT	94°C – 30sec	60°C – 30sec	72°C – 40sec	35	72°C – 5 min	WT: 256 bp
	Mutant allele	AGTGTGCCTGGCATGTGCAGACCTT	GGCAGAACTCGGATGCACAGATTGG						Floxed: 390 bp Delta: 566 bp
Tnfrsf11aKoba/Cre	WT allele Mutant allele	TGAAGGGTGACATCATCGTGGT ACTTCTCCATGGTAGCCTCC	AATAGGGGTGGGGTGATA AATAGGGGTGGGGTGATA	94°C – 30sec	60°C – 30sec	72°C – 30sec	35	72°C – 5 min	WT: 530 bp Mutant: 274 bp
Tnfrsf11aWafk/Cre	Mutant allele	AACCTGAGGATGTGAGGGACTA	GTCAAAGTCAGTGCGTTCAAAG	95°C – 30sec	58°C – 30sec	68°C – 60sec	35	72°C – 2 min	Mutant: 210 bp
VavDD/Cre	Mutant allele	GCCTGCATTACCGGTCGATGCAACGA	AATGGTGTTGCCGCGCCATCTGCCAC	95°C – 20sec	67°C – 20sec	72°C – 50sec	40	72°C – 2 min	Mutant: 700bp
CtfkCre		TTATTCCTTCCGCCAGGATG	TTGCTGTTATACTGCTTCTG	95°C – 30sec	55°C – 30sec	72°C – 60sec	35	72°C – 5 min	WT: 140 bp
			TAGTTTTTACTGCCAGACCG						Mutant: 300 bp

Extended Data Table 2.

Antibodies for Bone Histology

Fate-mapping models: *Flt3^{Cre};Rosa26$^{LSL-YFP}$,Cfs1r^{Cre};Rosa26$^{LSL-YFP}$ Csf1r^{MeriCreMer};Rosa26$^{LSL-YFP}$ and Tnfrsf11a^{Cre};Rosa26$^{LSL-YFP}$*								
		Conjugation	**Company**	**Catalog number**	**Concentration**	**Dilution**	**Staining Buffer**	**Incubating conditions**
Primary Antibody	Goat polyclonal anti-GFP	Biotin	Abcam	ab6658	1mg/mL	1::50	PBS/ 0.25%BSA/ 0.3% triton	4°C overnight (15hrs)
Secondary Antibody	Streptavidin	AlexaFluor488	Thermo Fisher Scientific	S-11223		1::100	PBS/ 0.25%BSA	2hrs at room temperature
Parabiosis								
		Conjugation	**Company**	**Catalog number**	**Concentration**	**Dilution**	**Staining Buffer**	**Incubating conditions**
Primary Antibodies	Goat polyclonal anti GFP Rabbit polyclonal anti-RFP	Biotin Unconugated	Abcam	ab6658 ab62341	1mg/mL	1::50 1::200	PBS/ 0.25%BSA/ 0.3% triton	4°C overnight (15hrs)
Secondary Antibodies	Streptavidin Goat anti-rabbit IgG	AlexaFluor488 AlexaFluor555	Thermo Fisher Scientific	S-11223 A21430	1mg/mL 2mg/mL	1::100 1::200	PBS/ 0.25%BSA	2hrs at room temperature
Bone marrow monocyte transfusions and transplants								
		Conjugation	**Company**	**Catalog number**	**Concentration**	**Dilution**	**Staining Buffer**	**Incubating conditions**

Fate-mapping models: *Flt3^{Cre};Rosa26$^{LSL-YFP}$,Cfs1r^{Cre};Rosa26$^{LSL-YFP}$ Csf1r^{MeriCreMer};Rosa26$^{LSL-YFP}$ and Tnfrsf11a^{Cre};Rosa26$^{LSL-YFP}$*								
		Conjugation	**Company**	**Catalog number**	**Concentration**	**Dilution**	**Staining Buffer**	**Incubating conditions**
Primary Antibodies	Goat polyclonal anti GFP Rabbit polyclonal anti-RFP	Biotin Unconugated	Abcam Rockland	ab6658 600–401-379	1mg/mL	1::50 1::200	PBS/ 0.25%BSA/ 0.3% triton	4°C overnight (15hrs)
Secondary Antibodies	Streptavidin Goat anti-rabbit IgG	AlexaFluor488 AlexaFluor555	Thermo Fisher Scientific	S-11223 A21430	1mg/mL 2mg/mL	1::100 1::200	PBS/ 0.25%BSA	2hrs at room temperature
EdU staining*								
		Conjugation	**Company**	**Catalog number**	**Concentration**	**Dilution**	**Staining Buffer**	**Incubating conditions**
Primary Antibody	Rat anti-mouse Tubulin	Unconjugated	Abcam	ab6160	1mg/mL	1::200	PBS/ 0.25%BSA/ 0.3% triton	4°C overnight (15hrs)
Secondary Antibody	Goat anti-rat IgG	AlexaFluor555	Thermo Fisher Scientific	A21434	2mg/mL	1::200	PBS/ 0.25%BSA	2hrs at room temperature

* After antibody staining sections were stained with the Click-it EdU Alexa Fluor 488 Imaging Assay kit, as described in methods.

Extended Data Table 3.

Antibodies for FACS

Antibody	**Clone**	**Fluorochrome**	**Company**	**Dilution**
CD3	145–2C11	bio	eBioscience	1/1000 (BM, Y, FL)
CD3	145–2C11	BV711	BD Pharmingen	1/100 (BM, SP, LV, K, BR) 1/400 (E)
CD3	145–2C11	APC-Cy7	BD Pharmingen	1/100 (BL)
CD3	145–2C11	PE	Bioiegend	1/100 (BM)
CD3	17A2	eF450	eBioscience	1/200 (BL)
CD11b	M1/70	bio	eBioscience	1/1000 (BM, Y, FL)
CD11b	M1/70	PE-Cy7	eBioscience	1/200 (BL, BM, SP, LV, K, BR, LN, E)
CD11b	M1/70	BV711	Bioiegend	1/200 (BM)
CD19	1D3	bio	eBioscience	1/500 (BM, Y, FL)
CD19	1D3	BV711	BD Pharmingen	1/100 (BM, SP, LV, K, BR) 1/200 (BL)
CD19	1D3	PE-Cy7	BD Pharmingen	1/400 (BL)
B220	RA3–6B2	bio	eBioscience	1/400 (BM,Y, FL)
Gr1	RB6–8C5	bio	eBioscience	1/1000 (BM,Y, FL)
NK1.1	PK136	bio	eBioscience	1/2000 (BM, Y, FL)
NKp46	29A1.4	BV711	BD Pharmingen	1/100 (BM, SP, LV, K, BR)
NKp46	29A1.4	AlexaFluor647	BD Pharmingen	1/200 (BL)
Ter119	Ter119	bio	eBioscience	1/500 (BM, Y, FL)
Ter119	Ter119	BV711	BD biosciences	1/200 (BM)

Antibody	Clone	Fluorochrome	Company	Dilution
CD11b	M1/70	PE	BD Pharmingen	1/1600 (BM)
CD11b	M1/70	APC-eF780	eBioscience	1/600 (SP, Y, FL, LV, LN, BR, P)
CD11c	N418	APC	eBioscience	1/150 (SP, BM,YS FL, LV, LN, BR, P)
CD45	30-F11	PE	eBioscience	1/150 (SP, BM, Y, FL, LV, LN, BR, P)
CD45	30-F11	APC-eF780	eBioscience	1/200 (Y, FL, P) 1/50 (BM, SP, LV, K) 1/100 (BR, LN, E)
CD45	30-F11	eF450	eBioscience	1/50 (BM)
CD48	HM48–1	BV421	BD Pharmingen	1/400 (BM,Y, FL)
CD48	HM48–1	APC	Bioiegend	1/100 (BM)
CD115	AFS98	APC	eBioscience	1/150 (SP, BM,Y, FL, LV, LN, BR, P)
CD115	AFS98	APC	Bioiegend	1/100 (BM)
CD115	AFS98	BV605	Bioiegend	1/200 (BL, BM, SP, LV, K, BR)
CD115	AFS98	PE	eBioscience	1/100 (SP, BM, LV, LN, BR, P)
CD117	2B8	PE-Cy7	eBioscience	1/3000 (Y, FL)
CD117	2B8	APC	eBioscience	1/400 (BM,Y, FL)
CD117	2B8	APC-Cy7	Bioiegend	1/100 (BM)
CD117	2B8	BV605	BD biosciences	1/100 (BM)
CD150	TC15–12F1	PE-Cy7	BioLegend	1/25 (Y, FL) 1/100 (BM)
F4/80	BM8	PE-Cy5	eBioscience	1/300 (SP, Y, FL, LV, LN, BR, P)
F4/80	BM8	eF450	eBioscience	1/100 (BM, BR, LN, E)
Gr-1	RB6–8C5	PECy5.5	eBioscience	1/3000 (SP, BM, Y, FL, LV, LN, BR, P)
Gr-1	RB6–8C5	eF450	eBioscience	1/1000 (Y, FL)
Gr-1	RB6–8C5	BV711	Bioiegend	1/100 (BM)
Ly6C	HK1.4	PerCpCy5.5	eBioscience	1/800 (Y, FL)
Ly6C	HK1.4	BV421	Bioiegend	1/200 (BL) 1/400 (SP, LV, K, BR)
Ly6C	HK1.4	BV510	Bioiegend	1/200 (BM)
Ly6C	HK1.4	AlexaFluor488	Bioiegend	1/50 (BM)
Ly6G	1A8	BV510	Bioiegend	1/100 (BM) 1/200 (Bi, LN) 1/400 (SP, LV, K, BR)
Ly6G	1A8	BV711	BD Pharmingen	1/200 (BM)
MHCII	M5/114.15.2	Alexa Fluor 700	eBioscience	1/150 (SP, BM,Y, FL, LV, LN, BR, P)
MHCII	M5/114.15.2	AlexaFluor700	Bioiegend	1/100 (BM) 1/200 (BL, SP, LV, K, BR)
Sca1	D7	PercpCy5.5	eBioscience	1/500 (BM,Y, FL)
Sca-1	D7	BV421	BD Pharmingen	1/200 (BM)
Sca-1	D7	BV711	Bioiegend	1/100 (BM)
Streptavidin		V500	BD Biosciences	1/800 (BM, Y, FL)
SigiecF	E50–2440	AlexaFluor647	BD Pharmingen	1/100 (BM, LN)

*BM: Bone marrow *BM: Bone marrow *SP: Spleen

* BL: Blood
* Y: Yolk sac
* FL: Fetal Liver
* LV: Liver
* LN: Lung
* BR: Brain
* P: PEC
* E: Epidermis
* K: Kidney

Supplementary Material

Refer to Web version on PubMed Central for supplementary material.

Acknowledgements

This work was supported by a NIH/NCI P30CA008748 MSKCC core grant, NIH/NIAID 1R01AI130345 and NIH/NHLBI R01HL138090 to F.G. and by the German Research Foundation (DFG) through FOR2033-A03, TRR127-A5, WA2837/6–1 and WA2837/7–1 to C.W. The authors thank Y. Kobayashi, J. Pollard, T. Graf, R. Stanley, J. Frampton[Author: Are Richard Stanley John Frampton two people? If not, please correct.], T. Boehm and J. Penninger for providing mouse strains, and the MSKCC molecular cytology core for preparation of histological samples. The authors are indebted to R. O'Reilly and F. Boulad for helpful suggestions. F.G. is grateful to G. Ruth for support. This study is dedicated to the memory of Lucile Crozet.

Reviewer information *Nature* thanks Roland Baron, Irving L. Weissmann and Mone Zaidi for their contribution to the peer review of this work.

References

1. Lacey DL et al. Osteoprotegerin ligand is a cytokine that regulates osteoclast differentiation and activation. Cell 93, 165–176 (1998). [PubMed: 9568710]
2. Kong YY et al. OPGL is a key regulator of osteoclastogenesis, lymphocyte development and lymph-node organogenesis. Nature 397, 315–323, doi:10.1038/16852 (1999). [PubMed: 9950424]
3. Dougall WC et al. RANK is essential for osteoclast and lymph node development. Genes Dev 13, 2412–2424 (1999). [PubMed: 10500098]
4. Hsu H et al. Tumor necrosis factor receptor family member RANK mediates osteoclast differentiation and activation induced by osteoprotegerin ligand. Proc Natl Acad Sci U S A 96, 3540–3545 (1999). [PubMed: 10097072]
5. Yoshida H et al. The murine mutation osteopetrosis is in the coding region of the macrophage colony stimulating factor gene. Nature 345, 442–444 (1990). [PubMed: 2188141]
6. Dai X-M et al. Targeted disruption of the mouse colony-stimulating factor 1 receptor gene results in osteopetrosis, mononuclear phagocyte deficiency, increased primitive progenitor cell frequencies, and reproductive defects. Blood 99, 111–120, doi:10.1182/blood.V99.1.111 (2002). [PubMed: 11756160]
7. Lomaga MA et al. TRAF6 deficiency results in osteopetrosis and defective interleukin-1, CD40, and LPS signaling. Genes Dev 13, 1015–1024 (1999). [PubMed: 10215628]
8. Tondravi MM et al. Osteopetrosis in mice lacking haematopoietic transcription factor PU.1. Nature 386, 81–84, doi:10.1038/386081a0 (1997). [PubMed: 9052784]
9. Takayanagi H et al. Induction and activation of the transcription factor NFATc1 (NFAT2) integrate RANKL signaling in terminal differentiation of osteoclasts. Dev Cell 3, 889–901 (2002). [PubMed: 12479813]
10. Lau RY & Guo X A review on current osteoporosis research: with special focus on disuse bone loss. J Osteoporos 2011, 293808, doi:10.4061/2011/293808 (2011).

11. Coccia PF et al. Successful bone-marrow transplantation for infantile malignant osteopetrosis. N Engl J Med 302, 701–708, doi:10.1056/NEJM198003273021301 (1980). [PubMed: 6986555]
12. Sorell M et al. Marrow transplantation for juvenile osteopetrosis. Am J Med 70, 1280–1287 (1981). [PubMed: 7015858]
13. Walker DG Bone resorption restored in osteopetrotic mice by transplants of normal bone marrow and spleen cells. Science 190, 784–785 (1975). [PubMed: 1105786]
14. Ballet JJ, Griscelli C, Coutris C, Milhaud G & Maroteaux P Bone-marrow transplantation in osteopetrosis. Lancet 2, 1137 (1977).
15. Nisbet NW, Menage J & Loutit JF Bone-marrow transplantation in osteopetrosis. Lancet 2, 1236 (1977).
16. Ash P, Loutit JF & Townsend KM Osteoclasts derived from haematopoietic stem cells. Nature 283, 669–670 (1980). [PubMed: 7354855]
17. Orchard PJ et al. Hematopoietic stem cell transplantation for infantile osteopetrosis. Blood 126, 270–276, doi:10.1182/blood-2015-01-625541 (2015). [PubMed: 26012570]
18. Frattini A et al. Rescue of ATPa3-deficient murine malignant osteopetrosis by hematopoietic stem cell transplantation in utero. Proceedings of the National Academy of Sciences of the United States of America 102, 14629–14634, doi:10.1073/pnas.0507637102 (2005).
19. Jotereau FV & Le Douarin NM The development relationship between osteocytes and osteoclasts: a study using the quail-chick nuclear marker in endochondral ossification. Dev Biol 63, 253–265 (1978). [PubMed: 346418]
20. Shalhoub V et al. Characterization of osteoclast precursors in human blood. Br J Haematol 111, 501–512 (2000). [PubMed: 11122091]
21. McGrath KE et al. Distinct Sources of Hematopoietic Progenitors Emerge before HSCs and Provide Functional Blood Cells in the Mammalian Embryo. Cell reports 11, 1892–1904, doi: 10.1016/j.celrep.2015.05.036 (2015). [PubMed: 26095363]
22. Gomez Perdiguero E et al. Tissue-resident macrophages originate from yolk-sac-derived erythro-myeloid progenitors. Nature 518, 547–551, doi:10.1038/nature13989 (2015). [PubMed: 25470051]
23. Maroteaux P & Lamy M [Pyknodysostosis]. Presse Med 70, 999–1002 (1962). [PubMed: 14470123]
24. Gelb BD, Shi GP, Chapman HA & Desnick RJ Pycnodysostosis, a lysosomal disease caused by cathepsin K deficiency. Science 273, 1236–1238 (1996). [PubMed: 8703060]
25. Taniguchi N et al. Stage-specific secretion of HMGB1 in cartilage regulates endochondral ossification. Molecular and cellular biology 27, 5650–5663, doi:10.1128/MCB.00130-07 (2007). [PubMed: 17548469]
26. Schulz C et al. A lineage of myeloid cells independent of Myb and hematopoietic stem cells. Science 336, 86–90, doi:10.1126/science.1219179 (2012). [PubMed: 22442384]
27. Mass E et al. Specification of tissue-resident macrophages during organogenesis. Science 353, doi: 10.1126/science.aaf4238 (2016).
28. Percin GI et al. CSF1R regulates the dendritic cell pool size in adult mice via embryo-derived tissue-resident macrophages. Nature communications 9, doi:10.1038/s41467-018-07685-x (2018).
29. Walker DG Osteopetrosis cured by temporary parabiosis. Science 180, 875 (1973). [PubMed: 4706681]

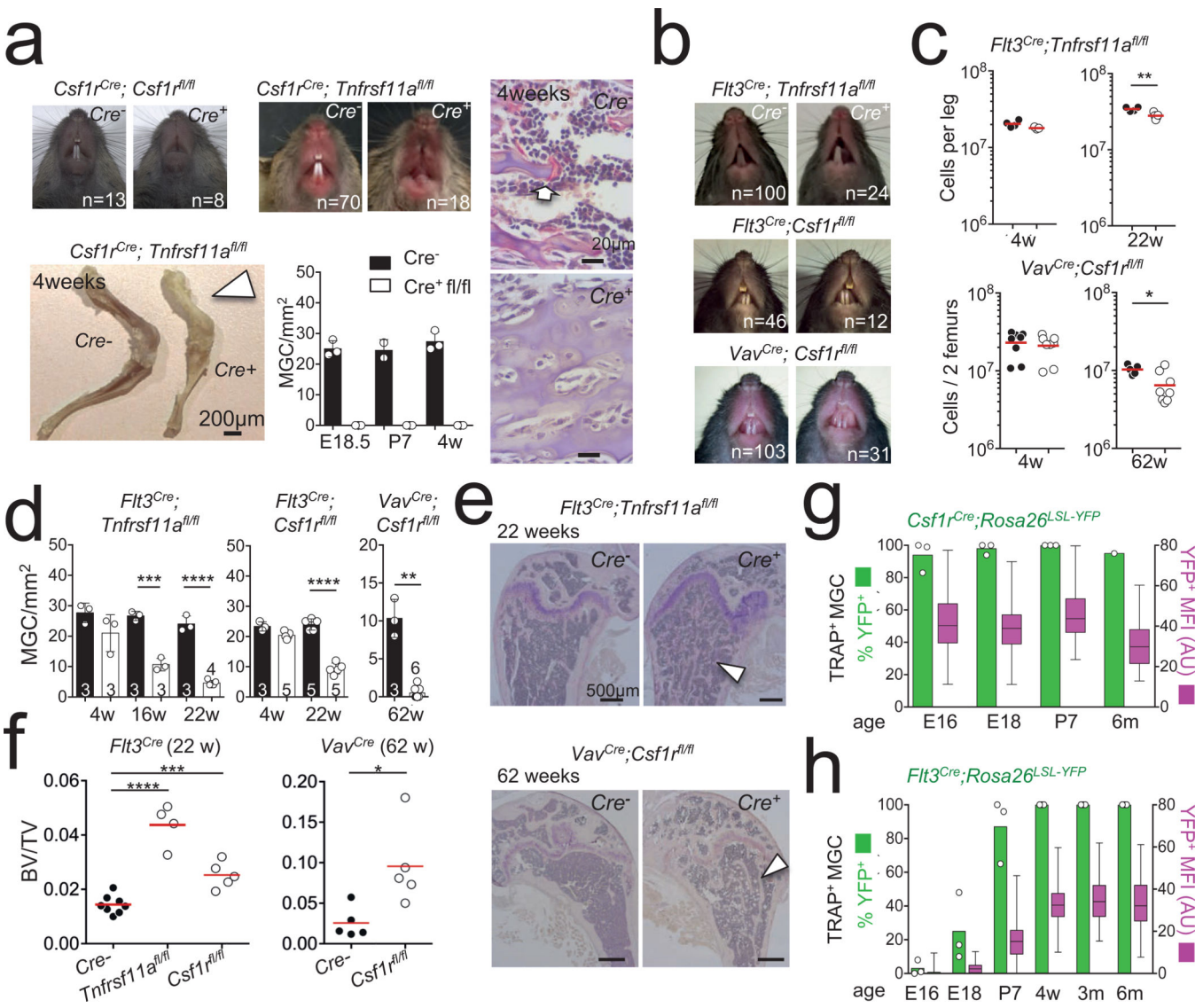

Fig. 1 |. HSC-derived precursors are dispensable for osteoclasts and bone development.

a, Representative photographs of teeth of three-to-four-week-old *Csf1r*^{Cre};*Csf1r*$^{fl/fl}$ mice (top left), *Csf1r*^{Cre};*Tnfrsf11a*$^{fl/fl}$ mice (top middle) and control littermates. Bottom left, representative photographs of leg bones from controls and *Csf1r*^{Cre};*Tnfrsf11a*$^{fl/fl}$ mice; white arrowhead highlights the lack of blood cells. Bottom middle, osteoclast numbers in E18.5, P7, and four-week-old *Csf1r*^{Cre};*Tnfrsf11a*$^{fl/fl}$ mice (n = 3) and control littermates (n = 3), and representative haematoxylin and TRAP staining of femur sections; the arrow indicates an osteoclast. **b**, Representative photographs of teeth of three-to-four-week-old *Flt3*^{Cre};*Tnfrsf11a*$^{fl/fl}$, *Flt3*^{Cre};*Csf1r*$^{fl/fl}$, *Vav*^{Cre};*Csf1r*$^{fl/fl}$ mice and littermates. **c**, Bone marrow CD45^{+} cell numbers in *Flt3*^{Cre};*Tnfrsf11a*$^{fl/fl}$ and control littermates at 4 (top left, n = 4 *Flt3*^{Cre};*Tnfrsf11a*$^{fl/fl}$, n = 3 control) and 22 weeks of age (top right; n = 4 *Flt3*^{Cre};*Tnfrsf11a*$^{fl/fl}$, n = 5 control) and *Vav*^{Cre};*Csf1r*$^{fl/fl}$ and control littermates at 4 (bottom left; n = 8 *Vav*^{Cre};*Csf1r*$^{fl/fl}$, n = 8 control) and 62 weeks of age (bottom right; n = 5 *Vav*^{Cre};*Csf1r*$^{fl/fl}$, n = 8 control), Cre^{-} black Cre^{+} white. **d**, Osteoclast counts in femurs from

Flt3^{Cre};*Tnfrsf11a*$^{fl/fl}$ (left), *Flt3*^{Cre};*Csf1r*$^{fl/fl}$ (middle) and *Vav*^{Cre};*Csf1r*$^{fl/fl}$ (right) mice and control littermates of the indicated ages, n numbers indicated on individual bars. **e**, Representative haematoxylin and TRAP staining of femur sections from 22-week-old *Flt3*^{Cre};*Tnfrsf11a*$^{fl/fl}$ mice (top), 62-week-old *Vav*$^{DD/Cre}$;*Csf1r*$^{fl/fl}$ mice (bottom) and control littermates. The white arrowhead points to trabecular bone. **f**, Quantitative analysis of bone volume/total volume of humerus or femurs from *Flt3*^{Cre};*Tnfrsf11a*$^{fl/fl}$ ($n = 4$), *Flt3*^{Cre};*Csf1r*$^{fl/fl}$ ($n = 5$) and control littermates ($n = 8$), and *Vav*^{Cre};*Csf1r*$^{fl/fl}$ ($n = 5$) mice and control littermates ($n = 5$) as determined by micro-CT. *P* values were determined by ANOVA. **g**, Expression and mean fluorescence intensity (MFI) of YFP in TRAP^{+} multinucleated cells from *Csf1r*^{Cre};*Rosa26*$^{LSL\text{-}YFP}$ mice at E16.5, E18.5, P7 and six months ($n = 3$ per time point). For MFI and percentages, at least 100 osteoclasts were quantified per time point and genotype. Box plots show the median, box edges show the first and third quartiles and whiskers show the minimum and maximum. **h**, Similar analysis as in **g**, for *Flt3*^{Cre};*Rosa26*$^{LSL\text{-}YFP}$ mice at E16.5, E18.5, P7, 4 weeks (4 wk), 3 months (3 m) and 6 months (6 m). Data are mean ± s.d.; dots in graphs represent individual independent biological replicates; *n* indicates the number of mice per group. Statistical significance was analysed with GraphPad Prism using unpaired two-tailed *t*-tests unless otherwise indicated. $*P < 0.05$, $**P < 0.01$, $***P < 0.001$ and $****P < 0.0001$.

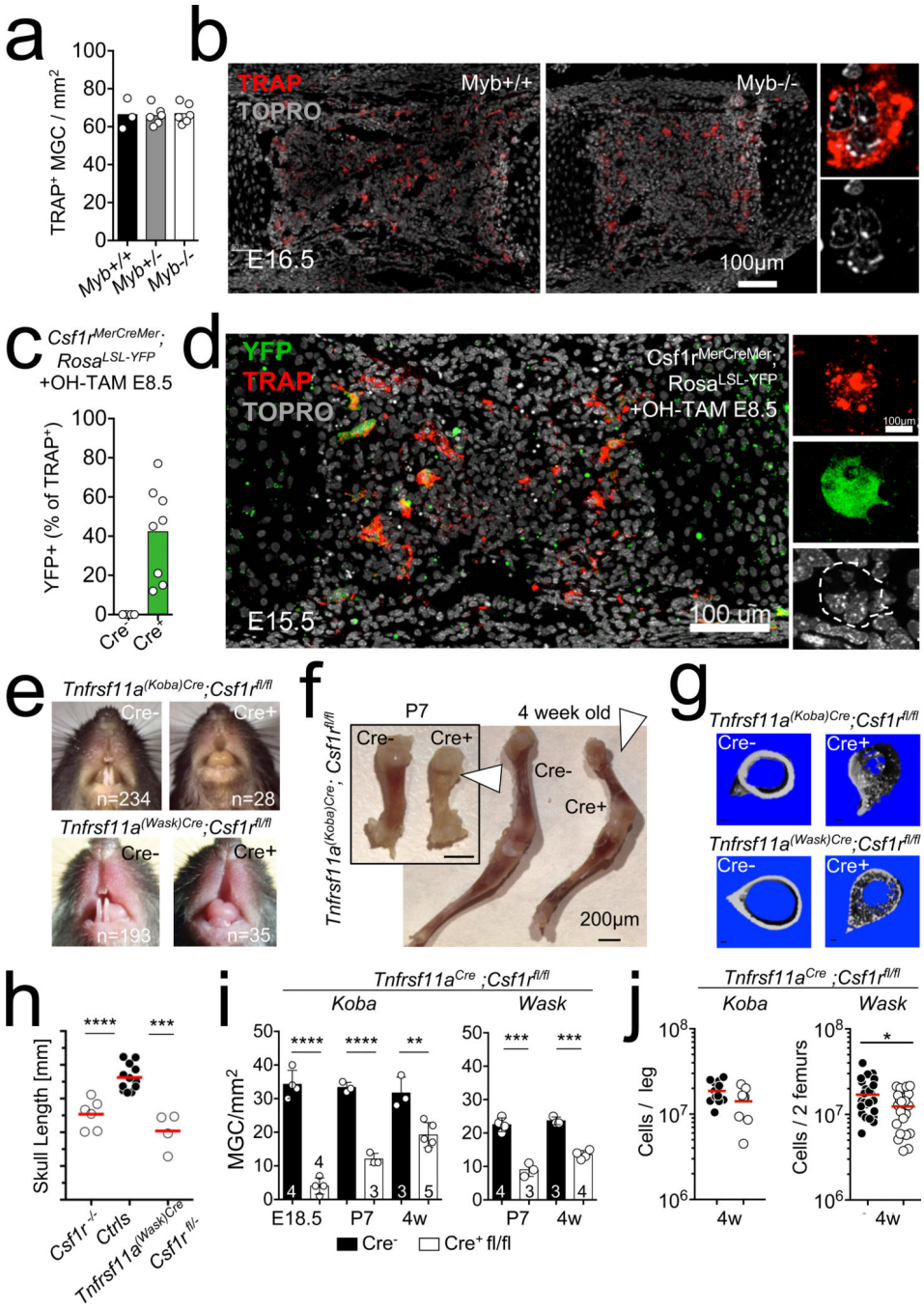

Fig. 2 |. EMP-derived osteoclasts are required for bone development.

a, MGC number in femur anlage ossification centres from E15.5–16.5 *Myb*$^{-/-}$ ($n = 6$) and littermate controls ($n = 3$). **b**, Representative confocal microscopy of frozen sections from the ossification centres in **a**, stained for TRAP and with TO-PRO-3 nuclear stain. **c**, Percentage of TRAP^{+} cells expressing YFP in femur anlage from E15.5 *Csf1r*$^{Mer\text{-}iCre\text{-}Mer}$;*Rosa26*$^{LSL\text{-}YFP}$ mice ($n = 8$) and Cre-negative controls ($n = 5$), pulsed at E8.5 with 4-OHT. **d**, Representative confocal microscopy of a sample from **c**. **e**, Representative teeth of cre^{+} *Tnfrsf11a*$^{Koba\text{-}Cre}$;*Csf1r*$^{fl/fl}$ (top) and *Tnfrsf11a*$^{Wask\text{-}Cre}$;*Csf1r*$^{fl/fl}$

mice (bottom) and cre^{-} control littermates. **f**, Leg bones from *Tnfrsf11a*^{Cre};*Csf1r*$^{fl/fl}$ mice (cre^{+}, $n = 6$) and control littermates (cre^{-}, $n = 6$) at P7 and 4 weeks of age. Arrowhead highlights the colour of an area of bone. **g**, Representative micro-CT scans of long bones from mice in **e** ($n = 6$ per genotype). **h**, Skull length from three-week-old *Csf1r*$^{-/-}$ ($n = 6$) control littermates ($n = 12$) and *Tnfrsf11a*$^{Wask\text{-}Cre}$;*Csf1r*$^{fl/fl}$ mice ($n = 4$), as determined by micro-CT. **i**, Osteoclast counts in bone sections from E18.5, P7 and three-to-four-week old *Tnfrsf11a*^{Cre};*Csf1r*$^{fl/fl}$ mice and littermate controls. **j**, Number of bone marrow CD45^{+} cells determined by flow cytometry of cells from four-week-old control (cre^{-}) littermates, *Tnfrsf11a*$^{Koba\text{-}Cre}$;*Csf1r*$^{fl/fl}$ ($n = 9$; $n = 13$ control) and *Tnfrsf11a*$^{Wask\text{-}Cre}$;*Csf1r*$^{fl/fl}$ ($n = 23$, $n = 27$ control) mice (cre^{+}). Data are mean ± s.d.; dots in graphs represent individual mice; n indicates the number of mice per group; unpaired two-tailed t-tests. *$P < 0.05$, **$P < 0.01$, ***$P < 0.001$ and ****$P < 0.0001$.

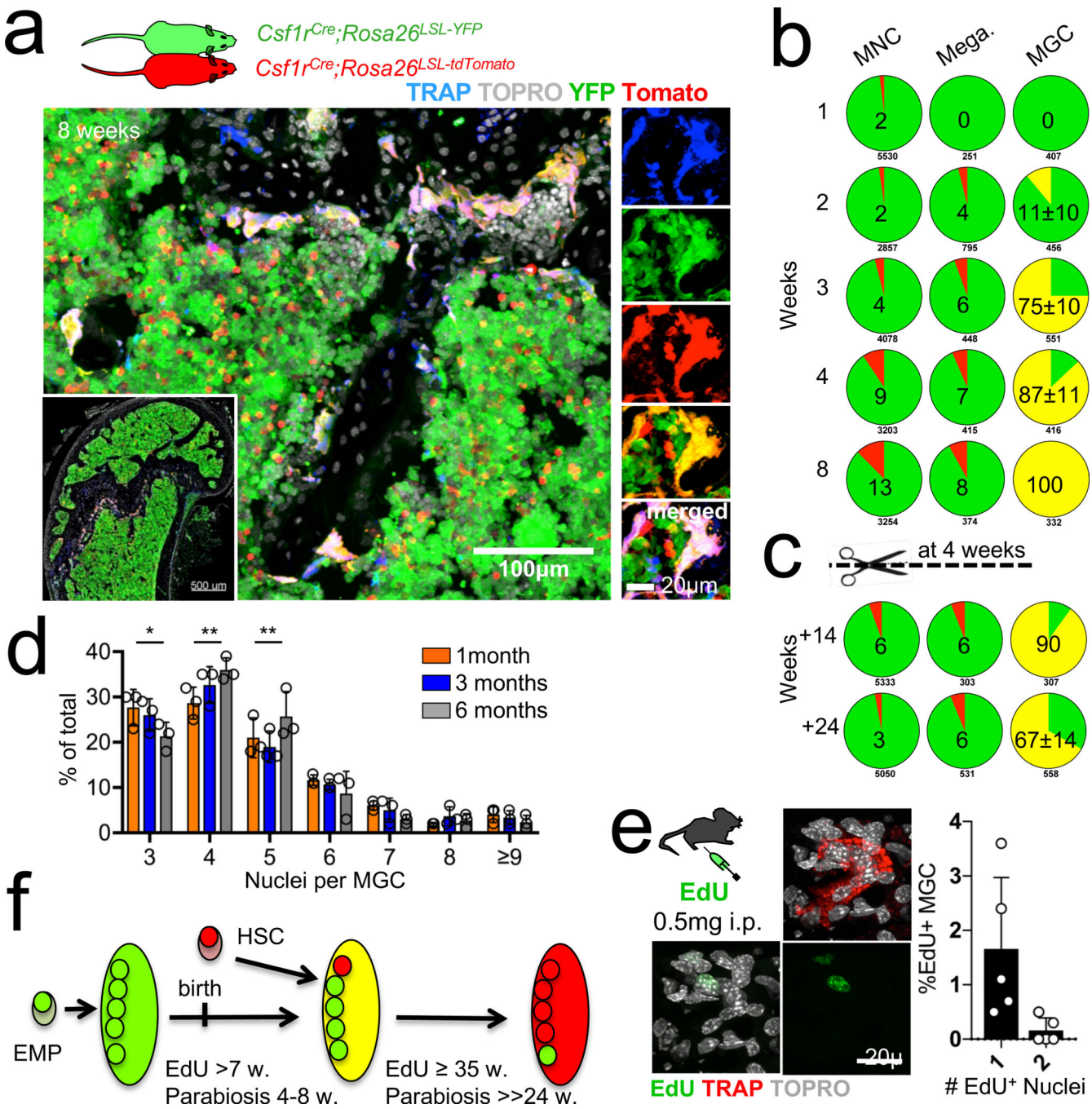

Fig. 3 |. In vivo dynamics of osteoclasts.

a, Parabiosis of *Csf1r*^{Cre};*Rosa26*$^{LSL\text{-}YFP}$ mouse surgically paired with a *Csf1r*^{Cre};*Rosa26*$^{LSL\text{-}tdTomato}$ partner for four-to-eight weeks. Representative confocal microscopy of frozen sections from the femur of a *Csf1r*^{Cre};*Rosa26*$^{LSL\text{-}YFP}$ partner stained with antibodies for tdTomato (red) and YFP (green), ELF 97 (blue) and TOPRO-3 (grey). n = 3. **b**, Pie graphs showing the percentage of tdTomato^{+} (red), YFP^{+} (green) and tdTomato^{+}YFP^{+} cells (yellow) among bone marrow mononuclear cells (MNC), megakaryocytes and multinuclear giant cells (MGC) from parabionts paired for the indicated time (n = 8). **c**,

Similar analysis as in **b** for parabionts separated after four weeks and analysed 14 and 24 weeks after separation ($n = 3$). **d**, Bar graph showing number of nuclei per $TRAP^+$ MGC in femurs from wild-type mice at one, three and six months of age ($n = 3$ mice per time point). **e**, Representative confocal microscopy of an EdU-labelled nucleus in a $TRAP^+$ osteoclast (left) and histogram showing the percentage of $TRAP^+$ osteoclasts with EdU-labelled nuclei and the number of labelled nuclei per cell 72 h after intravenous pulse-labelling with EdU ($n = 5$ mice). **f**, A model for development and maintenance of osteoclast syncytia. Data are mean ± s.d.; dots in graphs represent individual mice; n indicates the number of mice per group; two-way ANOVA with Tukey's multiple comparisons test $*P \leq 0.05$ and $**P \leq 0.005$.

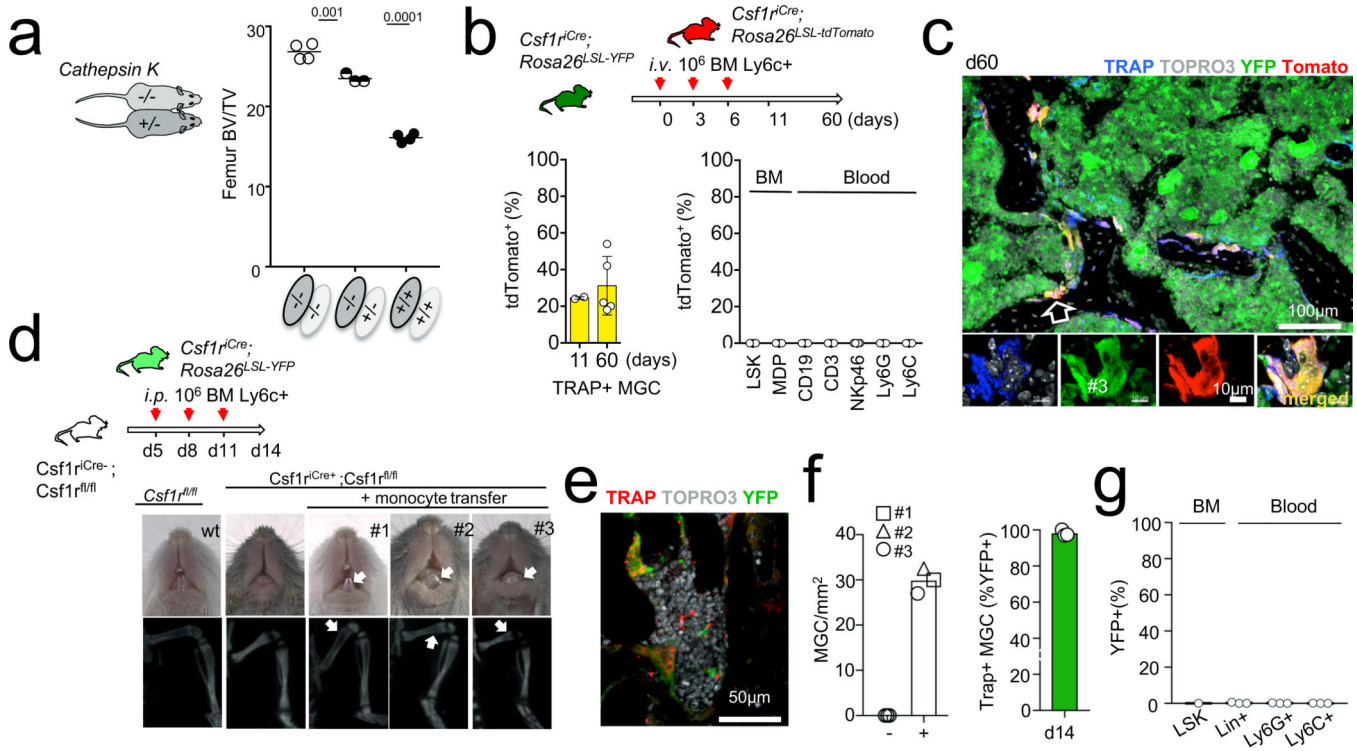

Fig. 4 |. Rescue of osteopetrosis.

a, Bone volume/total volume for femurs from 10-week-old cathepsin $K^{-/-}$ mice ($n = 3$) after six weeks parabiosis with cathepsin $K^{+/-}$ mice and from positive ($n = 4$) and negative ($n = 4$) control parabionts, analysed by von Kossa staining. **b**, Monocyte transfer. Histograms represent percentage of tdTomato$^+$ cells among bone TRAP$^+$ MGCs from *Csf1r*^{Cre};*Rosa26*$^{LSL\text{-}YFP}$ recipients analysed by confocal microscopy (left) 11 days ($n = 2$) and 60 days ($n = 5$) after intravenous transfer at six weeks of age of 3×10^6 Ly6C$^+$ bone marrow cells from *Csf1r*^{Cre};*Rosa26*$^{LSL\text{-}tdTomato}$ donors, and percentages of tdTomato$^+$ cells among bone marrow precursors and blood leukocytes, analysed by flow cytometry after 60 days ($n = 5$, right). **c**, Representative high-power confocal microscopy of the femur of a recipient mouse 60 days after intravenous transfer (from **b**), stained with antibodies for tdTomato and YFP, ELF97 phosphatase substrate and TOPRO-3. **d**, Representative photographs of teeth (top) and CT scan of leg bones from *Csf1r*^{cre};*Csf1r*$^{fl/fl}$ mice ($n = 3$) transferred with monocytic cells from *Csf1r*^{Cre};*Rosa26*$^{LSL\text{-}YFP}$ donors at P5, P8 and P11, and from wild-type and non-transferred *Csf1r*^{cre};*Csf1r*$^{fl/fl}$ controls. Arrows indicate the presence of teeth eruption (top panels) and bone marrow cavity (bottom panels). **e**, Representative confocal microscopy of a femur from mouse no. 3 in **d**, stained with YFP antibody and with ELF97 and TOPRO-3. **f**, Number of TRAP$^+$ osteoclasts in bone sections from mice in **d** and non-transferred controls (left), and percentage of YFP$^+$ TRAP$^+$ cells in transferred mice. The different symbols represent individual mice. Mean values for three sections per mouse. At least 100 osteoclasts were quantified per mouse. **g**, Percentages of YFP$^+$ cells among bone marrow precursors and blood leukocytes in the recipient mice (from **d**) at the time of analysis. Data are mean ± s.d.; dots in graphs represent individual mice; *n*

indicates the number of mice per group; ANOVA with Tukey's multiple comparisons test. *** $P < 0.001$ and **** $P < 0.0001$.